



RESEARCH ARTICLE

## [2.2.2.2]Paracyclophanetetraenes (PCTs): cyclic structural analogues of poly(*p*-phenylene vinylene)s (PPVs) [version 1; peer review: awaiting peer review]

Matthias Pletzer<sup>1,2</sup>, Felix Plasser <sup>3</sup>, Martina Rimmel <sup>1,2</sup>, Martin Heeney<sup>1,2</sup>, Florian Glöcklhofer <sup>1,2</sup>

<sup>1</sup>Department of Chemistry, Imperial College London, London, W12 0BZ, UK

<sup>2</sup>Centre for Processable Electronics, Imperial College London, London, W12 0BZ, UK

<sup>3</sup>Department of Chemistry, Loughborough University, Loughborough, LE11 3TU, UK

**V1** First published: 23 Sep 2021, 1:111  
<https://doi.org/10.12688/openreseurope.13723.1>  
Latest published: 23 Sep 2021, 1:111  
<https://doi.org/10.12688/openreseurope.13723.1>

### Open Peer Review

**Reviewer Status** AWAITING PEER REVIEW

Any reports and responses or comments on the article can be found at the end of the article.

### Abstract

**Background:** Poly(*p*-phenylene vinylene)s (PPVs) and [2.2.2.2]paracyclophanetetraene (PCT) are both composed of alternating  $\pi$ -conjugated *para*-phenylene and vinylene units. However, while the former constitute a class of  $\pi$ -conjugated polymers that has been used in organic electronics for decades, the latter is a macrocycle that only recently revealed its potential for applications such as organic battery electrodes. The cyclic structure endows PCT with unusual properties, and further tuning of these may be required for specific applications. **Methods:** In this article, we adopt an approach often used for tuning the properties of PPVs, the introduction of alkoxy (or alkylthio) substituents at the phenylene units, for tuning the optoelectronic properties of PCT. The resulting methoxy- and methylthio-substituted PCTs, obtained by Wittig cyclisation reactions, are studied by UV-vis absorption, photoluminescence, and cyclic voltammetry measurements, and investigated computationally using the visualisation of chemical shielding tensors (VIST) method. **Results:** The measurements show that substitution leads to slight changes in terms of absorption/emission energies and redox potentials while having a pronounced effect on the photoluminescence intensity. The computations show the effect of the substituents on the ring currents and chemical shielding and on the associated local and global (anti)aromaticity of the macrocycles, highlighting the interplay of local and global aromaticity in various electronic states. **Conclusions:** The study offers interesting insights into the tuneability of the properties of this versatile class of  $\pi$ -conjugated macrocycles.

## Keywords

macrocycles,  $\pi$ -conjugated macrocycles, paracyclophanetetraene, PCT, poly(*p*-phenylene vinylene), PPV, visualisation of chemical shielding tensors, VIST, aromaticity, antiaromaticity, rotamers, Wittig reaction, photoluminescence, cyclic voltammetry



This article is included in the [Excellence Gateway](#).

**Corresponding author:** Florian Glöcklhofer ([f.glocklhofer@imperial.ac.uk](mailto:f.glocklhofer@imperial.ac.uk))

**Author roles:** **Pletzer M:** Investigation, Methodology, Validation, Writing – Original Draft Preparation, Writing – Review & Editing; **Plasser F:** Data Curation, Formal Analysis, Funding Acquisition, Investigation, Methodology, Project Administration, Resources, Validation, Visualization, Writing – Original Draft Preparation, Writing – Review & Editing; **Rimmele M:** Investigation, Validation; **Heeney M:** Funding Acquisition, Project Administration, Supervision, Writing – Review & Editing; **Glöcklhofer F:** Conceptualization, Data Curation, Funding Acquisition, Methodology, Project Administration, Resources, Supervision, Visualization, Writing – Original Draft Preparation, Writing – Review & Editing

**Competing interests:** No competing interests were disclosed.

**Grant information:** This research was financially supported by the European Union's Horizon 2020 research and innovation programme under the Marie Skłodowska-Curie grant agreement No 796024. This work was also supported by funding from the Austrian Science Fund (FWF), project number J 4463, and from the Engineering and Physical Sciences Research Council (EPSRC), grant EP/V048686/1. *The funders had no role in study design, data collection and analysis, decision to publish, or preparation of the manuscript.*

**Copyright:** © 2021 Pletzer M *et al.* This is an open access article distributed under the terms of the [Creative Commons Attribution License](#), which permits unrestricted use, distribution, and reproduction in any medium, provided the original work is properly cited.

**How to cite this article:** Pletzer M, Plasser F, Rimmele M *et al.* **[2.2.2]Paracyclophanetetraenes (PCTs): cyclic structural analogues of poly(*p*-phenylene vinylene)s (PPVs) [version 1; peer review: awaiting peer review]** Open Research Europe 2021, 1:111 <https://doi.org/10.12688/openreseurope.13723.1>

**First published:** 23 Sep 2021, 1:111 <https://doi.org/10.12688/openreseurope.13723.1>

## Introduction

Poly(*p*-phenylene vinylene)s (**PPVs**) are among the best investigated  $\pi$ -conjugated polymers<sup>1,2</sup>. They are composed of alternating *para*-phenylene and vinylene units and usually feature substituents attached to the  $\pi$ -conjugated backbone to modify their optoelectronic and dissolution properties. Most frequently, alkoxy substituents are attached to the phenylene units, but the corresponding alkylthio-substituted **PPVs** have also been reported<sup>3</sup>. The alkyl part of the substituents (often a linear or branched alkyl chain) is intended to improve the solubility, while the purpose of the oxygen or sulfur atom linking the alkyl part to the backbone is to modify the optoelectronic properties, mainly through their positive mesomeric effect.

[2.2.2.2]Paracyclophanetetraene (**PCT**) can be seen as a cyclic structural analogue of unsubstituted **PPV** (Figure 1). This  $\pi$ -conjugated macrocycle, first synthesized in the 1970s<sup>4</sup>, was recently rediscovered by us and has proven to be a capable battery electrode material<sup>5</sup>. The excellent redox and charge storage properties of **PCT** have been attributed to ring currents and voids enabled by the cyclic structure of the molecule, suggesting that the optoelectronic properties of **PCT** and **PPV** differ significantly, despite their structural similarity. In contrast to the polymers, the vinylene units in **PCT** must adopt a *cis*-configuration; no end groups are present that may affect the properties.

The aim of the work presented here was to synthesize and study **PCT** derivatives with alkoxy and alkylthio substituents at the phenylene units, in analogy to the well-investigated substituted **PPVs**. In contrast to **PPV**, **PCT** dissolves well in organic solvents also without substituents with linear or branched alkyl chains. Thus, simple methyl groups were selected as the alkyl part of the substituents. When studying the properties of the resulting methoxy- and methylthio-substituted **PCT** derivatives, we were particularly interested in the

effect of the substituents on the ring currents, having recently reported the drastic effects of the introduction of ester groups (at the vinylene units) on these currents<sup>6</sup>.

## Results and discussion

### Synthesis

Unsubstituted **PCT** can be synthesized by a Wittig cyclisation reaction in yields of 10% to 15% using [1,4-phenylenebis(methylene)]bis(triphenylphosphonium) dibromide (**P1**) and terephthalaldehyde (**P2**) as the cyclisation precursors<sup>4,5</sup>. Aiming for an analogous synthesis of methoxy- and methylthio-substituted **PCT** derivatives, we first synthesized the substituted Wittig cyclisation precursors **O-P1**, **S-P1**, and **S-P2** (Figure 2): The phosphonium salts **O-P1** and **S-P1** were synthesized via the same route, but while 1,4-dimethoxybenzene (**O-2**) for the synthesis of **O-P1** is readily available from commercial suppliers, the corresponding methylthio-substituted compound 1,4-bis(methylthio)benzene (**S-2**) for the synthesis of **S-P1** was obtained by a copper-catalysed conversion of 4-bromothioanisole (**S-1**) in dimethyl sulfoxide (DMSO)<sup>7</sup>. Compounds **O-2** and **S-2** were then bromomethylated by adapting our previously reported procedures to these substrates<sup>3</sup>. The reactions yielded compounds **O-3** and **S-3** in yields of 52% and 87%, respectively. In the final step, **O-3** and **S-3** were reacted with triphenylphosphine (PPh<sub>3</sub>) in boiling toluene, affording **O-P1** and **S-P1** as white solids in good yields. In contrast, the dialdehyde **S-P2** was synthesized by slightly adapting published procedures for the bromination of **P2** in the first step and nucleophilic aromatic substitution with sodium methanethiolate (NaSCH<sub>3</sub>) in the second step<sup>8,9</sup>.

The phosphonium salts **O-P1** and **S-P1** were then reacted with terephthalaldehyde (**P2**) in dimethylformamide (DMF) at a low temperature of -40 °C (Figure 3). As for the synthesis of **PCT**<sup>5</sup>, lithium methoxide dissolved in anhydrous methanol (MeOH) was used as the base for these Wittig cyclisation

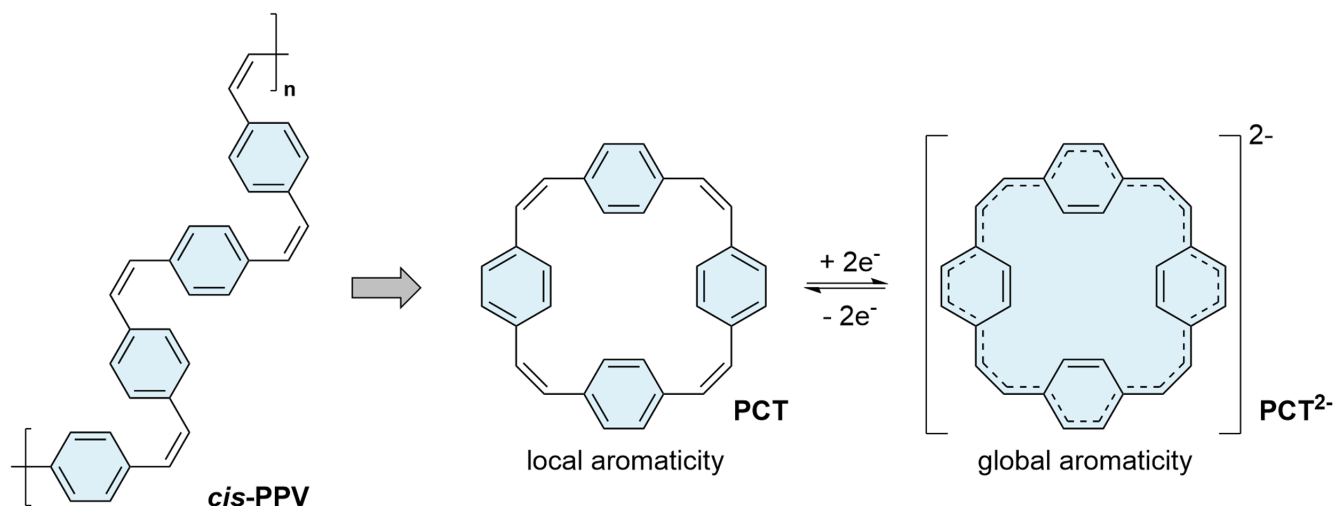


**Figure 1.** [2.2.2.2]Paracyclophanetetraene (**PCT**) as a cyclic structural analogue of *cis*-poly(*p*-phenylene vinylene) (*cis*-**PPV**) (left); reversible two-electron reduction and aromaticity switching of **PCT** (right).

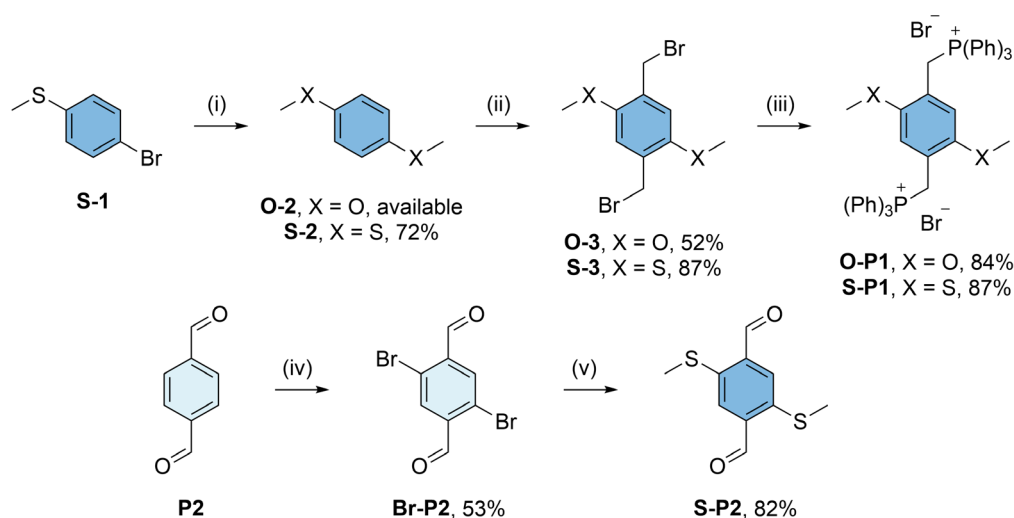


**Figure 2.** Synthesis of methoxy- and methylthio-substituted Wittig cyclisation precursors **O-P1**, **S-P1**, and **S-P2**. Reaction conditions: (i) CuI, Cu(OAc)<sub>2</sub>, dimethyl sulfoxide (DMSO), 135 °C; (ii) paraformaldehyde, HBr in acetic acid, 1,4-dioxane (X = O) / formic acid (X = S), 80 °C; (iii) PPh<sub>3</sub>, toluene, 120 °C; (iv) N-bromosuccinimide (NBS), conc. H<sub>2</sub>SO<sub>4</sub>, 60 °C; (v) NaSCH<sub>3</sub>, dimethylformamide (DMF), r.t..

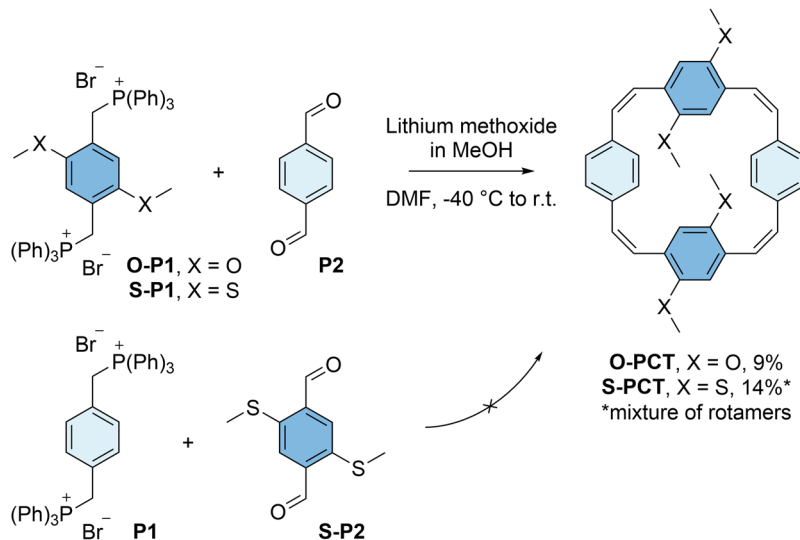


**Figure 3.** Synthesis of methoxy- and methylthio-substituted [2.2.2]paracyclophanetetraenes **O-PCT** and **S-PCT** by Wittig cyclisation reactions of precursors **O-P1/S-P1** and **P2** (top). The analogous reaction of precursors **P1** and **S-P2** did not yield the product (bottom).

reactions. The base was added slowly using a syringe pump, affording the macrocycles **O-PCT** and **S-PCT** in yields of 9% and 14%, respectively, after work-up and purification by gel permeation chromatography (GPC). In contrast, placing the methylthio substituents on the aldehyde precursor instead of the phosphonium salt, reacting *p*-xylylenebis(triphenylphosphonium bromide) (**P1**) with precursor **S-P2** under the same reaction conditions, did not afford any **S-PCT**, presumably due to a less favourable *cis/trans* ratio of the vinylene units formed in this Wittig reaction (the electronic character of the

precursors can influence the ratio). The reaction of **S-P1** and **S-P2** to obtain the macrocycle with substituents on all four phenylene units has also been attempted but did not give the desired product.

#### Conformation

<sup>1</sup>H NMR spectra of **S-PCT** recorded at room temperature and 50 °C indicated the presence of two rotamers that could not be separated (see Figure 4 for an illustration of the two rotamers). A rotamer ratio of approximately 10:1, which corresponds to a

free energy difference of about 6 kJ/mol, was determined from the integrals. In contrast, the  $^1\text{H}$  NMR spectrum of **O-PCT** did not show the presence of rotamers, indicating a lower energy barrier for the rotation of the phenylene units with methoxy substituents than with methylthio substituents.

To test these assumptions, computations were carried out to estimate the energy barrier for the interconversion of the two rotamers. Indeed, a barrier of only 45 kJ/mol was found for **O-PCT**. According to the Eyring equation, this corresponds to an interconversion time of about 10  $\mu\text{s}$ , which is well below the time scale relevant to NMR. Both rotamers are very similar in energy, with the  $C_s$  rotamer 3.2 kJ/mol below the  $C_2$  rotamer, suggesting that both are present at room temperature. **S-PCT**, on the other hand, showed a significantly enhanced barrier of 94 kJ/mol with an associated interconversion time well above one hour. The  $C_2$  rotamer was found to be more stable by 16.6 kJ/mol, which is similar but somewhat larger than the free energy difference deduced from experiment (see above). The difference in behaviour between the two molecules can be understood by the fact that the methylthio groups are bulkier, causing steric strain for the transition state and the  $C_s$  rotamer. Taking the neutral  $C_2$  rotamer as an example, we

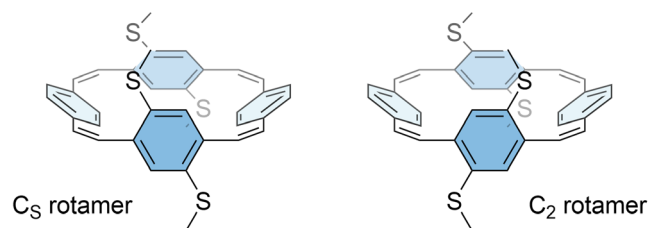


**Figure 4.** Illustration of the two rotamers of **S-PCT**, classified according to their idealised symmetry properties. The computed energy barrier for interconversion is 94 kJ/mol.

find that the two C-O bonds in **O-PCT** are 1.35 and 1.39 Å in length whereas the C-S bonds in **S-PCT** measure 1.77 and 1.81 Å.

#### UV-vis absorption and photoluminescence

UV-vis absorption measurements in  $\text{CHCl}_3$  solution (Figure 5, solid lines) showed slightly blueshifted absorption maxima for **O-PCT** ( $\lambda_{\text{abs,max}} = 304$  nm) and **S-PCT** ( $\lambda_{\text{abs,max}} = 293$  nm) compared to **PCT** ( $\lambda_{\text{abs,max}} = 306$  nm). The second absorption peak in the spectrum of **S-PCT** ( $\lambda_{\text{abs}} = 283$  nm) may be attributed to the presence of two rotamers. Photoluminescence (PL) measurements of the solutions (Figure 5, dashed lines) showed a significant increase in PL intensity upon introduction of the substituents, particularly upon introduction of the methoxy substituents. Similar sensitivity to the substitution pattern for the PL intensity were also found for the related ester-substituted molecules and can be tentatively assigned to symmetry breaking in the excited state, lifting the selection rules for the formally symmetry-forbidden  $S_1$  state<sup>6</sup>, see, e.g., reference 10 for a discussion of the underlying physics. In contrast to the absorption maxima, the PL maxima of **O-PCT** ( $\lambda_{\text{PL,max}} = 502$  nm) and **S-PCT** ( $\lambda_{\text{PL,max}} = 481$  nm) were found to be redshifted compared to **PCT** ( $\lambda_{\text{PL,max}} = 468$  nm), thus increasing their Stokes shifts from 1.40 eV for **PCT** to 1.61/1.65 eV for **O-PCT/S-PCT**. It is worth noting that the Stokes shifts of the linear **PCT** analogue containing 4 phenylene-vinylene units ( $\lambda_{\text{abs,max}} = 396$  nm;  $\lambda_{\text{PL,max}} = 463$  nm)<sup>11</sup>, of alkoxy-substituted **PPV** ( $\lambda_{\text{abs,max}} = 502$  nm;  $\lambda_{\text{PL,max}} = 558$  nm)<sup>12</sup>, and alkylthio-substituted **PPV** ( $\lambda_{\text{abs,max}} = 453$  nm;  $\lambda_{\text{PL,max}} = 527$  nm)<sup>3</sup> are all well below 0.5 eV, highlighting the dramatic effect of the cyclic conjugation. Indeed, the large Stokes shifts of the substituted and unsubstituted **PCTs**, resulting in almost no spectral overlap between absorption and emission, can be seen as a signature of excited-state aromaticity, cf. references 6 and 13. Thus, the spectra suggest that symmetry breaking is only a dynamic effect accounting for a minor perturbation of excited-state aromaticity (see below for a further discussion).

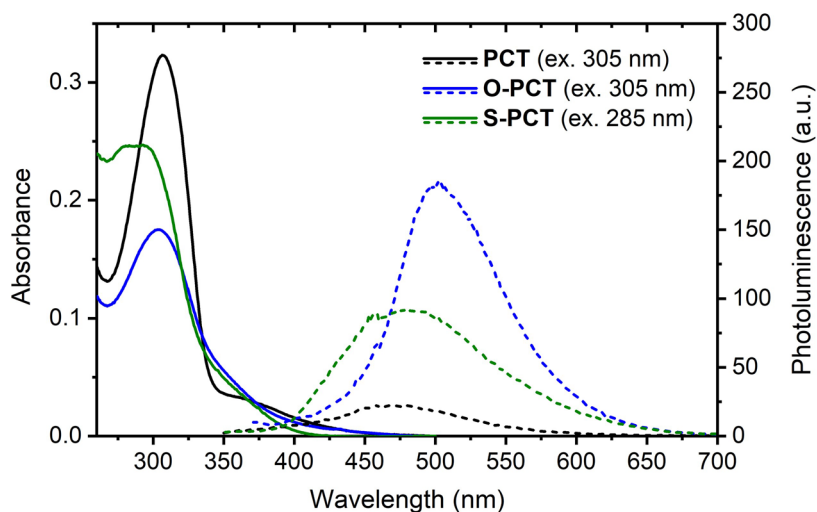


**Figure 5.** UV-vis absorption (solid lines) and photoluminescence spectra (dashed lines) of the macrocycles in  $\text{CHCl}_3$  solution (approx. 5  $\mu\text{M}$ ). The excitation wavelengths for recording the photoluminescence (PL) spectra are shown in brackets.

## Redox potentials

Cyclic voltammetry measurements of the macrocycles in 1,2-dichloroethane (DCE) and dimethylformamide (DMF) (Figure 6) were carried out to determine the redox potentials vs. ferrocene/ferrocene<sup>+</sup> (Fc/Fc<sup>+</sup>) in two different solvents. As a general trend, the redox potentials for both the reductions and oxidations shifted to lower values upon introduction of the substituents, with a slightly larger shift observed for the introduction of the methoxy substituents. This can be explained by the electron-donating character of the substituents.

In DCE, the redox potential for the first reduction wave shifted from -2.26 V for **PCT** to -2.34 V for **S-PCT** and -2.37 V for **O-PCT**. For **S-PCT**, a second reduction wave was observed at -2.50 V. The redox potential for the first oxidation wave shifted from 0.81 V for **PCT** to 0.73 V for **S-PCT** and 0.61 V for **O-PCT**. For **S-PCT**, the first derivative of the measure-

ment indicated further oxidations at 0.79 V and 1.08 V. For **O-PCT**, a second and third oxidation wave were observed at 0.73 V and 1.03 V, respectively.

In DMF, the redox potential for the first reduction wave showed a shift from -2.09 V for **PCT** to -2.26 V for **S-PCT** and -2.27 V for **O-PCT**. No further reduction waves were observed in this solvent. The redox potential for the first oxidation wave shifted from 0.76 V for **PCT** to 0.62 V for **S-PCT** and 0.58 V for **O-PCT**. A second oxidation wave was observed at 0.83 V for **S-PCT** and 0.74 V for **O-PCT**.

Computations place the potentials for concerted two-electron reduction in DCE at -2.28, -2.40, and -2.35 V for **PCT**, **O-PCT**, and **S-PCT**, respectively, suggesting that the experimental reduction potentials refer to two-electron processes. Potentials for two-electron oxidation are placed at 0.89, 0.75, and 0.98 V for the three molecules. Considering that the values for **O-PCT** and **S-PCT** are considerably higher than the measured first oxidation potentials, this suggests that oxidation proceeds via one-electron processes.

## Ring currents and chemical shielding

To study the effect of the methoxy and methylthio substituents on the magnetic properties (ring currents and chemical shielding) and on the associated local and global (anti)aromaticity of the macrocycles, the visualisation of chemical shielding tensors (VIST) method<sup>14</sup>, which is based on the nucleus independent chemical shift<sup>15</sup>, was used. As explained previously<sup>6,14</sup>, VIST allows the visualisation of local variations in aromaticity and antiaromaticity in the context of the molecular structure by showing the chemical shielding tensor components using a representation of blue (shielded, aromatic) or red (deshielded, antiaromatic) dumbbells. Each tensor component relates to ring currents in a plane perpendicular to it.

The VIST plots of **O-PCT** and **S-PCT** in the neutral  $S_0$  and  $T_1$  states as well as in the doubly charged  $S_0$  states are provided in Figure 7 and Figure 8, respectively. Shielding tensors were computed at the centre of the ring to probe global ring currents as well as 1 Å off the centre of the phenylene units to probe their local aromaticity. Both rotamers of the macrocycles were analysed. The corresponding VIST plots of **PCT** are provided in our previous work<sup>6</sup>. The substituents are seen to have little effect on the magnetic properties of the neutral  $S_0$  state. As in our previous analysis of **PCT**, the main component of the chemical shielding tensors located 1 Å off the planes of the phenylene units is shielded and almost perpendicular to the planes, indicating their local aromaticity. At the centre of the macrocycle, the tensor component perpendicular to the plane of the macrocycle is slightly deshielded, possibly indicating weak global antiaromaticity of the macrocyclic [4n]  $\pi$ -electron system.

In contrast to the  $S_0$  state, the magnetic properties of the neutral  $T_1$  state of **O-PCT** and **S-PCT** differ significantly from those of **PCT**. The VIST plots of **PCT** in the  $T_1$  state indicate strong aromatic macrocyclic currents (and perturbed local aromaticity).

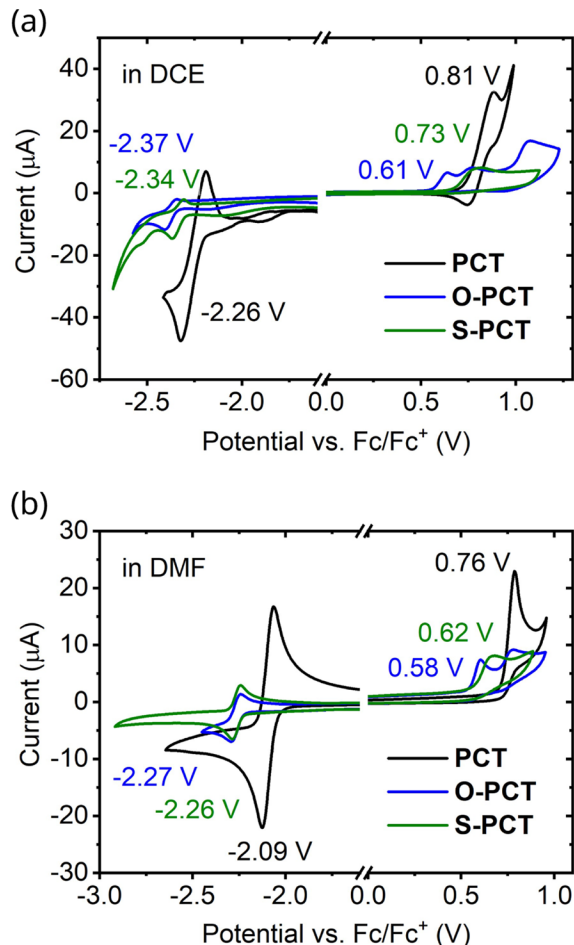


**Figure 6.** Cyclic voltammograms of the macrocycles in 1,2-dichloroethane (DCE) and dimethylformamide (DMF) recorded using a glassy carbon working electrode, a platinum mesh auxiliary electrode, and a silver wire quasi-reference electrode (QRE) at a scan rate of 0.1 V s<sup>-1</sup>. 0.1 M tetrabutylammonium hexafluorophosphate (NBu<sub>4</sub>PF<sub>6</sub>) was used as the supporting electrolyte.

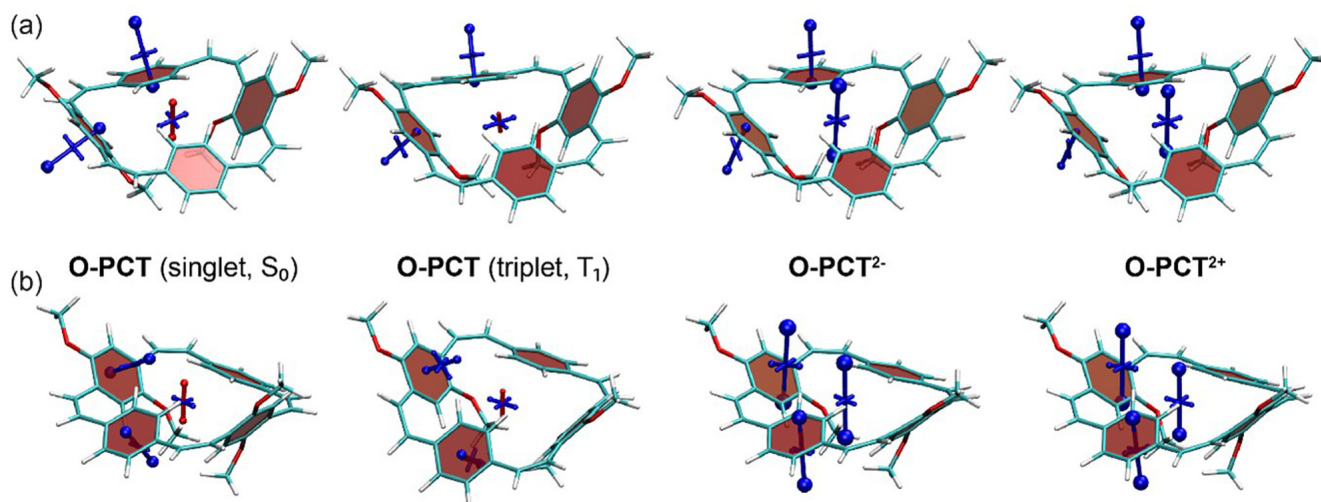


**Figure 7.** VIST plots for the rotamers (a)  $C_2$  and (b)  $C_s$  of **O-PCT** (classified according to their idealised symmetry properties) in different charge and spin states. Shielded (aromatic) tensor components are shown in blue, deshielded (antiaromatic) tensor components in red. Each tensor component relates to ring currents in a plane perpendicular to it.

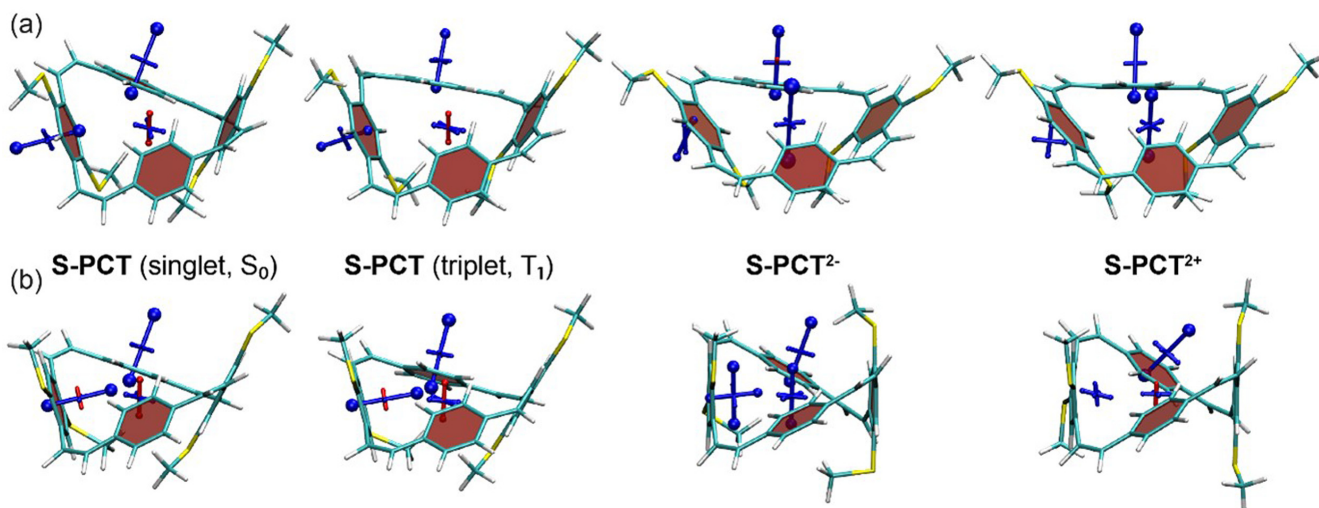


**Figure 8.** VIST plots for the rotamers (a)  $C_2$  and (b)  $C_s$  of **S-PCT** (classified according to their idealised symmetry properties) in different charge and spin states. Shielded (aromatic) tensor components are shown in blue, deshielded (antiaromatic) tensor components in red. Each tensor component relates to ring currents in a plane perpendicular to it.

This macrocyclic Baird aromaticity is obliterated by the introduction of the substituents; as the  $S_0$  state, the neutral  $T_1$  states of **O-PCT** and **S-PCT** are dominated by the local aromaticity of the phenylene units. To explain this phenomenon, we analysed the electronic structure in more detail by computing the natural difference orbitals (NDOs)<sup>16</sup> between the  $S_0$  and  $T_1$  states of the  $C_2$  rotamer of **O-PCT** as an example. The NDOs, shown on the upper left in **Figure 9**, reveal that in the  $T_1$  state the symmetry is broken, and the excitation is localised on one side of the molecule. More specifically, the excitation is centred

around one of the vinyl groups, which is strongly twisted out of plane. Following the arguments in Ref. 17, it can be understood that Baird aromaticity would only be achieved if the transition occurred between delocalised orbitals in a cyclically conjugated structure. Next, we were interested whether similar symmetry breaking occurs for the  $S_1$  state. Therefore, the  $S_1$  state was optimised, and the NDOs obtained are shown on the lower left in **Figure 9**. In contrast to the  $T_1$  state, the excitation in the  $S_1$  state is evenly delocalised over the whole macrocycle. Closer inspection shows that both NDOs possess

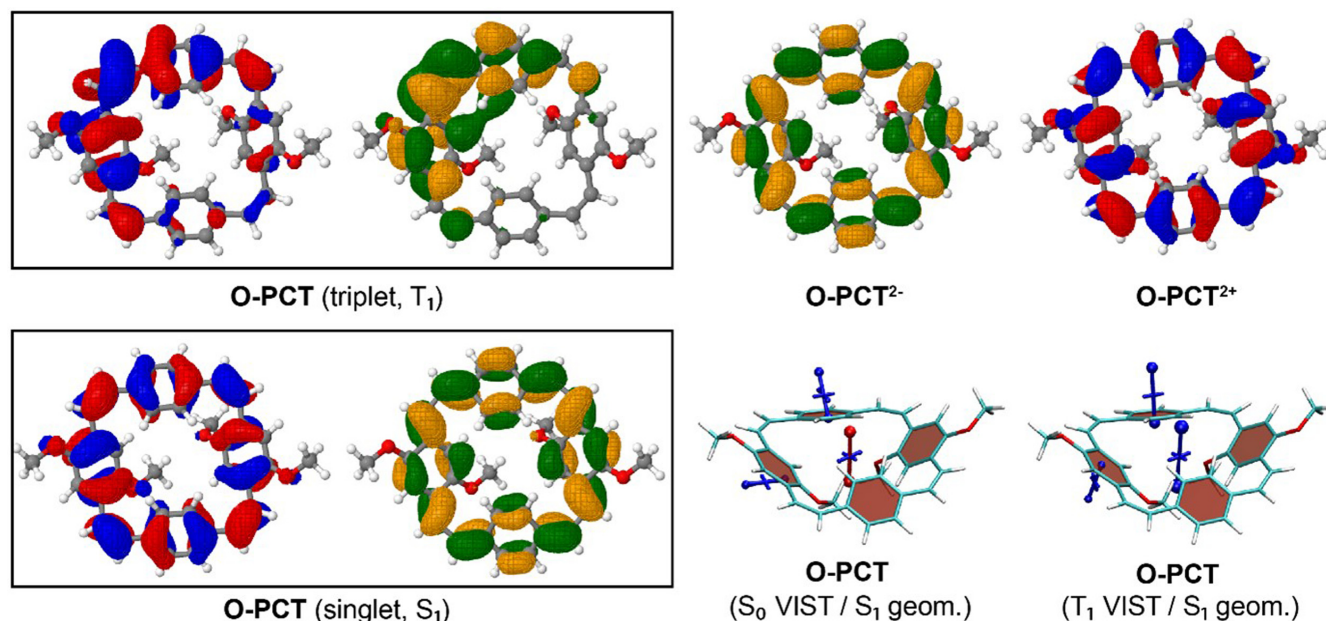


**Figure 9.** Dominant natural difference orbitals (NDOs) (blue/red for electron detachment; green/orange for attachment) for different electronic states of O-PCT ( $C_2$  rotamer) and VIST plots for the  $S_0$  and  $T_1$  states at the  $S_1$  geometry.

12 nodal planes, corresponding to the quasidegenerate HOMO and LUMO of the parent [24]annulene structure. The excitation occurs between these quasidegenerate orbitals, which is the signature of excited-state aromaticity within the MO picture<sup>17</sup> and is, thus, consistent with the large Stokes shift observed in the measurements. The computation of shielding tensors in the  $S_1$  state is not routinely possible. Therefore, we have computed VIST plots of the  $S_0$  and  $T_1$  states at the  $S_1$  geometry instead (Figure 9, bottom right). These show enhanced antiaromaticity and aromaticity compared to the VIST plots at the geometries optimized for the respective states, further confirming that the  $S_1$  geometry facilitates delocalisation.

Differently to the  $T_1$  state, the VIST plots of the doubly charged states of O-PCT and S-PCT (Figure 7 and Figure 8) indicate similarly strong macrocyclic aromaticity as observed for PCT<sup>2-</sup> and PCT<sup>2+</sup> with the exception of the  $C_s$  rotamer of S-PCT<sup>2+</sup> for which the VIST plot does not indicate any macrocyclic currents. In all other cases, the main component of the chemical shielding tensors at the phenylene units are tilted and almost perpendicular to the plane of the macrocycle, indicating strong perturbation of the local aromaticity by macrocyclic currents. The central shielding tensors also indicate the strong macrocyclic currents. To exemplify the change in electronic structure, we present the NDOs of the  $C_2$  rotamer of O-PCT (Figure 9, upper right). The relevant attachment NDO for the dianion as well as the detachment NDO for the dication are both evenly delocalised over the entire macrocycle. More specifically, they are of similar shape as the  $S_1$  NDOs, possessing the 12 nodal planes corresponding to the quasidegenerate [24]annulene frontier orbitals. Revisiting the  $C_s$  rotamer of S-PCT<sup>2+</sup>, we find that its relevant orbitals do not possess

the required cyclically delocalised structure, thus explaining the lack of aromaticity.

In summary, we find that O-PCT and S-PCT possess similar electronic structure as the parent PCT molecule. But similarly to our previously discussed ester-substituted molecules<sup>6</sup>, we find that due to their lower symmetry they are further removed from the underlying idealised antiaromatic [24]annulene structure. The large Stokes shifts seen in the UV/vis absorption and PL spectra (Figure 5) are consistent with excited-state aromaticity, as seen for the optimised  $S_1$  state of O-PCT in Figure 9. On the other hand, we tentatively assign the enhanced photoluminescence activity of the substituted molecules to an increased propensity for symmetry breaking, which is seen explicitly in the  $T_1$  optimised structure and probably also plays a role for the  $S_1$  state in terms of structural fluctuations. However, a full ab initio simulation of the resulting spectra is out of the scope of this work.

## Conclusions

Our study shows that methoxy- and methylthio-substituted PCT derivatives can be obtained by Wittig cyclisation reactions of substituted [1,4-phenylenebis(methylene)]bis(triphenylphosphonium) dibromides and terephthalaldehyde, in similar yields as reported for the synthesis of unsubstituted PCT. The required substituted Wittig cyclisation precursors can be obtained in good yields via a two/three-step procedure. Placing substituents on the terephthalaldehyde precursor did not yield the macrocycles in our attempts.

While the energy barrier for the rotation of the methoxy-substituted phenylene units in O-PCT was found to allow a rapid

interconversion of the two rotamers, the significantly higher energy barrier for the rotation of the methylthio-substituted phenylene units in **S-PCT** resulted in distinct  $^1\text{H}$  NMR signals that can be assigned to the two rotamers. Computations supported this finding, highlighting that the interconversion barrier in **S-PCT** is more than twice the barrier in **O-PCT**, increasing the expected interconversion time from 10  $\mu\text{s}$  to well over one hour. The larger barrier was related to the bulkier nature of the methylthio substituents when compared to the methoxy substituents.

The introduction of the substituents was also found to alter the optoelectronic properties of **PCT**. In particular, the maximum photoluminescence (PL) intensity of **O-PCT** was found to be approximately eight times higher than for **PCT**, a feature that we assign to dynamic excited-state symmetry breaking and the associated lifting of selection rules. While the PL maxima were found to be redshifted, the UV-vis absorption maxima of **O-PCT** and **S-PCT** were slightly blueshifted compared to **PCT**, thus increasing the overall Stokes shifts to above 1.5 eV, which is more than three times the value of the linear **PPV** analogues. Furthermore, the electron-donating character of the substituents leads to a shift of the redox potentials to lower values, as confirmed by cyclic voltammetry measurements in two different solvents along with computations. This can be an interesting feature for tuning the properties for applications such as organic battery electrodes and further confirms the high tuneability of the properties of this compound class.

In the neutral and most of the doubly charged singlet states of **O-PCT** and **S-PCT**, the ring currents and chemical shielding do not differ significantly from those of **PCT** in the same states, according to our computational investigation using the visualisation of chemical shielding tensors (VIST) method. However, in the neutral  $T_1$  state, the macrocyclic Baird aromaticity observed in the VIST plots of **PCT** is obliterated by the introduction of the substituents and the associated breaking of the symmetry; the molecules are dominated by the local aromaticity of the phenylene units.

In summary, the study expands the set of available [2.2.2]cyclophanetetraenes and offers further insights into the tuneability of the properties of this versatile compound class.

## Methods

### Synthetic methods

Reagents and solvents for the synthesis were purchased from commercial suppliers and used without further purification, including compounds **S-1** (Sigma-Aldrich, product number 196525), **O-2** (Sigma-Aldrich, product number D131350), **P1** (Alfa Aesar, product number A18241.14), and **P2** (Sigma-Aldrich, product number 808617). Purification by recycling preparative GPC was carried out on a LaboACE LC-5060 (Japan Analytical Industry Co., Tokyo, JAPAN) system equipped with a JAIGEL-2HR column and a TOYDAD800-S detector.

**1,4-Bis(methylthio)benzene (S-2):** Synthesis adapting a published procedure<sup>7</sup>. 4-Bromothioanisole (**S 1**) (508 mg, 2.5

mmol, 1.0 equiv.), CuI (119 mg, 0.63 mmol, 0.25 equiv.) and  $\text{Cu}(\text{OAc})_2$  (908 mg, 5.0 mmol, 2.0 equiv.) were added to an oven-dried vial, purged with nitrogen and sealed before adding 8 mL DMSO. The suspension was heated to 135 °C for 36 hours before cooling to room temperature (r.t.) and adding 40 mL  $\text{Et}_2\text{O}$ . The orange suspension was filtered off and washed with cold  $\text{H}_2\text{O}$  before extracting the filtrate with  $\text{Et}_2\text{O}$  (3x), drying the organic phase with  $\text{Na}_2\text{SO}_4$  and removing the solvent under reduced pressure. Product **S-2** was purified by column chromatography using hexane/ $\text{Et}_2\text{O}$  (10:1), yielding an off-white, wax-like solid (305 mg, 1.8 mmol, 72%).  $^1\text{H}$  NMR (400 MHz,  $\text{CDCl}_3$ ):  $\delta$  7.20 (s, 4H), 2.47 (s, 6H) ppm; in accordance with the literature<sup>7</sup>.

**2,5-Bis(bromomethyl)-1,4-dimethoxybenzene (O-3):** Synthesis adapting a procedure used for the bromomethylation of 1,4-dihexyloxybenzene<sup>3</sup>. 1,4-Dimethoxybenzene (**O-2**) (691 mg, 5.0 mmol, 1.0 equiv.) and paraformaldehyde (901 mg, 30 mmol, 6.0 equiv.) were suspended in 20 mL 1,4-dioxane. 8.0 mL HBr (30% in acetic acid) was added dropwise and the reaction was heated to 80 °C for 24 hours. The white suspension was slowly cooled to r.t., allowing the product to crystallise as a white solid. The solid was filtered off, washed twice with  $\text{H}_2\text{O}$  and recrystallised from acetonitrile (MeCN), yielding product **O-3** as white needles (837 mg, 2.6 mmol, 52%).  $^1\text{H}$  NMR (400 MHz,  $\text{CDCl}_3$ ):  $\delta$  6.87 (s, 2H), 4.54 (s, 4H), 3.87 (s, 6H) ppm; in accordance with the literature<sup>18</sup>.

**2,5-Bis(bromomethyl)-1,4-bis(methylthio)benzene (S-3):** Synthesis adapting a procedure used for the bromomethylation of related substrates<sup>3</sup>. 1,4-Bis(methylthio)benzene (**S-2**) (375 mg, 2.2 mmol, 1.0 equiv.) and paraformaldehyde (264 mg, 8.8 mmol, 4.0 equiv.) were dissolved in 20 mL formic acid while heating to 80 °C. 3.1 mL HBr (30% in acetic acid) were added and the reaction was stirred at 80 °C for 1 hour. Paraformaldehyde (264 mg, 8.8 mmol, 4.0 equiv.) and 3.1 mL HBr (30% in acetic acid) were added three more times in intervals of 1 hour; the reaction was then stirred at 80 °C overnight using a magnetic stirrer. The white suspension was slowly cooled to r.t., allowing the product to crystallise as an off-white solid. Product **S-3** was isolated by filtering and washing with MeOH (685 mg, 1.9 mmol, 87%).  $^1\text{H}$  NMR (400 MHz,  $\text{CD}_2\text{Cl}_2$ ):  $\delta$  7.28 (s, 2H), 4.63 (s, 4H), 2.52 (s, 6H) ppm.  $^1\text{H}$  NMR (400 MHz,  $\text{CDCl}_3$ ):  $\delta$  7.26 (s, 2H, overlaps with solvent peak), 4.61 (s, 4H), 2.52 (s, 6H) ppm;  $^{13}\text{C}\{^1\text{H}\}$  NMR (101 MHz,  $\text{CDCl}_3$ ):  $\delta$  137.2, 136.0, 129.5, 31.1, 16.7 ppm. HRMS ( $m/z$ ):  $[\text{M}]^+$  calcd for  $\text{C}_{10}\text{H}_{12}\text{S}_2\text{Br}_2$ : 353.8742, found: 353.8733 (APCI).

**[(2,5-dimethoxy-1,4-phenylene)bis(methylene)]bis(triphenylphosphonium) dibromide (O-P1):** Substrate **O-3** (713 mg, 2.2 mmol, 1.0 equiv.) and  $\text{PPh}_3$  (2.02 g, 7.7 mmol, 3.5 equiv.) were suspended in 7.5 mL anhydrous toluene in a sealed vial under nitrogen and heated to 120 °C overnight. The white precipitate was filtered and washed with toluene and  $\text{Et}_2\text{O}$ . Product **O-P1** was isolated as a white solid (1.56 g, 1.8 mmol, 84%).  $^1\text{H}$  NMR (400 MHz,  $\text{CDCl}_3$ ):  $\delta$  7.79 – 7.73 (m, 6H), 7.73 – 7.61 (m, 24H), 6.96 (d,  $J = 1.9$  Hz, 2H), 5.23 (d,  $J = 12.8$  Hz, 4H), 2.97 (s, 6H) ppm.  $^{31}\text{P}\{^1\text{H}\}$  NMR (162 MHz,  $\text{CDCl}_3$ ):  $\delta$

21.82 ppm. HRMS ( $m/z$ ):  $[M-2Br]^{2+}$  calcd for  $C_{46}H_{42}Br_2O_2P_2$ : 344.1330, found: 344.1325 (ESI).

**[(2,5-bis(methylthio)-1,4-phenylene)bis(methylene)]bis(triphenylphosphonium) dibromide (S-P1):** Substrate **S-3** (605 mg, 1.7 mmol, 1.0 equiv.) and  $PPh_3$  (1.34 g, 5.1 mmol, 3.0 equiv.) were suspended in 25 mL anhydrous toluene in a sealed vial under nitrogen and heated to 120 °C overnight. The white precipitate was filtered and washed with toluene and  $Et_2O$ . Product **S-P1** was isolated as a white solid (1.30 g, 1.5 mmol, 87%) after triturating in boiling *n*-butanol for 1.5 h for further purification.  $^1H$  NMR (400 MHz,  $CDCl_3$ ):  $\delta$  7.82 – 7.74 (m, 6H), 7.73 – 7.59 (m, 24H), 7.13 (d,  $J = 2.1$  Hz, 2H), 5.52 (d,  $J = 12.5$  Hz, 4H), 1.71 (s, 6H) ppm.  $^{31}P\{^1H\}$  NMR (162 MHz,  $CDCl_3$ ):  $\delta$  22.00 ppm. HRMS ( $m/z$ ):  $[M-2Br]^{2+}$  calcd for  $C_{46}H_{42}Br_2P_2S_2$ : 360.1101, found: 360.1111 (ESI).

**2,5-Dibromoterephthalaldehyde (Br-P2):** Synthesis adapting a published procedure<sup>8</sup>. Terephthalaldehyde (**P2**) (8.05 g, 60 mmol, 1.0 equiv.) was dissolved in 80 mL conc.  $H_2SO_4$  at 60 °C. *N*-Bromosuccinimide (NBS) (23.5 g, 132 mmol, 2.2 equiv.) was added in small portions over 30 min. The reaction was then stirred for 3 hours at 60 °C before cooling to r.t. and pouring onto ice. The white precipitate was washed with aq.  $NaHCO_3$  and brine before being recrystallised from  $CHCl_3$ . **Br-P2** was isolated as off-white crystals (9.30 g, 31.9 mmol, 53%).  $^1H$  NMR (400 MHz,  $CDCl_3$ ):  $\delta$  10.35 (s, 2H), 8.16 (s, 2H) ppm; in accordance with the literature<sup>19</sup>.

**2,5-Bis(methylthio)terephthalaldehyde (S-P2):** Synthesis adapting a published procedure<sup>9</sup>. **Br-P2** (992 mg, 3.4 mmol, 1.0 equiv.) was dissolved in 70 mL DMF before adding  $NaSCH_3$  (498 mg, 7.1 mmol, 2.1 equiv.) at r.t. The dark red solution was stirred for 10 minutes and then poured into 250 mL 1M HCl, forming an orange precipitate. The mixture was extracted with  $CHCl_3$  (3x), the organic phase dried with  $Na_2SO_4$  and the solvent removed under reduced pressure. The crude product was recrystallised from MeCN, yielding **S-P2** as an orange solid (630 mg, 2.8 mmol, 82%).  $^1H$  NMR (400 MHz,  $CDCl_3$ ):  $\delta$  10.41 (s, 2H), 7.80 (s, 2H), 2.57 (s, 6H) ppm; in accordance with the literature<sup>9</sup>.

**Methoxy-substituted [2.2.2.2]paracyclophanetetraene O-PCT:** Wittig cyclisation precursor **O-P1** (1.19 g, 1.4 mmol, 1.0 equiv.) and terephthalaldehyde (**P2**) (188 mg, 1.4 mmol, 1.0 equiv.) were dissolved in 70 mL anhydrous DMF under nitrogen, purged with nitrogen for 5 min and cooled to -40 °C using an MeCN/dry ice bath. Lithium methoxide (159 mg, 4.2 mmol, 3.0 equiv.) was dissolved in 18 mL anhydrous MeOH by sonication, purged with nitrogen for 2 minutes (purge carefully to avoid precipitation) and added to the reaction over 9 hours using a syringe pump. The rate of addition was adjusted to maintain a faint red colour of the solution. After complete addition of the base, the reaction was stirred overnight, using a magnetic stirrer, while warming to r.t. The resulting suspension was poured into  $H_2O$  and extracted with  $Et_2O$  (3x), the organic

phase dried with  $Na_2SO_4$  and the solvent removed in vacuo. The obtained solid was dissolved  $CH_2Cl_2$  and flashed over silica using  $CH_2Cl_2$  as the eluent until the solvent ran clear (to remove the Wittig reaction side product triphenylphosphine oxide (TPPO)). The crude product was purified by recycling preparative GPC using  $CHCl_3$  as the eluent, yielding **O-PCT** as a yellow oil that crystallised slowly over time (32 mg, 0.06 mmol, 9%).  $^1H$  NMR (400 MHz,  $CDCl_3$ ):  $\delta$  7.08 (s, 8H), 6.72 (s, 4H), 6.58 (d,  $J = 12.2$  Hz, 4H), 6.52 (d,  $J = 12.1$  Hz, 4H), 3.55 (s, 12H) ppm.  $^{13}C\{^1H\}$  NMR (101 MHz,  $CDCl_3$ ):  $\delta$  151.1, 136.0, 130.8, 128.8, 127.0, 126.2, 113.4, 56.3 ppm. HRMS ( $m/z$ ):  $[M]^+$  calcd for  $C_{36}H_{32}O_4$ : 528.2301, found: 528.2301 (ESI).

**Methylthio-substituted [2.2.2.2]paracyclophanetetraene S-PCT:** Wittig cyclisation precursor **S-P1** (1.00 g, 1.14 mmol, 1.0 equiv.) and terephthalaldehyde (**P2**) (153 mg, 1.14 mmol, 1.0 equiv.) were dissolved in 35 mL anhydrous DMF under nitrogen, purged with nitrogen for 5 min and cooled to -40 °C using an MeCN/dry ice bath. Lithium methoxide (130 mg, 3.4 mmol, 3.0 equiv.) was dissolved in 9 mL anhydrous MeOH by sonication, purged with nitrogen for 2 minutes (purge carefully to avoid precipitation) and added to the reaction over 9 hours using a syringe pump. The rate of addition was adjusted to maintain a faint red colour of the solution. After complete addition of the base, the reaction was stirred overnight while warming to r.t. The resulting suspension was poured into  $H_2O$  and extracted with  $Et_2O$  (3x), the organic phase dried with  $Na_2SO_4$  and the solvent removed in vacuo. The obtained solid was dissolved  $CH_2Cl_2$  and flashed over silica using  $CH_2Cl_2$  as the eluent until the solvent ran clear (to remove the Wittig reaction side product triphenylphosphine oxide (TPPO)). The crude product was purified by recycling preparative GPC using  $CHCl_3$  as the eluent, yielding **S-PCT** as an orange solid (48 mg, 0.08 mmol, 14%).  $^1H$  NMR measurements (including measurements at elevated temperature) suggest that the product is a mixture of two rotamers (ratio approx. 10:1, determined from  $^1H$  NMR integrals). *Main rotamer:*  $^1H$  NMR (400 MHz,  $CDCl_3$ ):  $\delta$  6.97 (s, 4H), 6.95 (s, 8H), 6.63 (d,  $J = 12.0$  Hz, 4H), 6.57 (d,  $J = 12.0$  Hz, 4H), 2.14 (s, 12H) ppm.  $^{13}C\{^1H\}$  NMR (101 MHz,  $CDCl_3$ ):  $\delta$  137.0, 135.6, 134.2, 131.5, 129.0, 128.2, 127.0, 16.0 ppm.  $^1H$  NMR (400 MHz,  $CDCl_3$ , 50 °C):  $\delta$  7.00 (s, 4H), 6.95 (s, 8H), 6.65 (d,  $J = 11.9$  Hz, 4H), 6.58 (d,  $J = 11.9$  Hz, 4H), 2.14 (s, 12H) ppm. *Minor rotamer:*  $^1H$  NMR (400 MHz,  $CDCl_3$ ): 7.00 (s, 4H), 6.98 (s, 8H), 6.58 (s, 8H), 2.22 (s, 12H) ppm.  $^1H$  NMR (400 MHz,  $CDCl_3$ , 50 °C):  $\delta$  7.03 (s, 4H), 6.99 (s, 8H), 6.58 (s, 8H), 2.21 (s, 12H) ppm. HRMS ( $m/z$ ):  $[M+H]^+$  calcd for  $C_{36}H_{32}S_4$ : 593.1460, found: 593.1444 (APCI).

#### Measurement methods and instrumentation

NMR spectra were recorded in  $CDCl_3$  solution at 400 MHz for  $^1H$ , 101 MHz for  $^{13}C$ , and 162 MHz for  $^{31}P$  on a Bruker AV-400 spectrometer. High-resolution mass spectrometry (HRMS) was carried out on systems from Thermo Scientific (Thermo Scientific Q-Exactive/Dionex Ultimate 3000) for atmospheric pressure chemical ionization (APCI) and Waters (Waters

LCT Premier (ES-ToF)/Acquity i-Class) for electrospray ionization (ESI). While the Thermo Scientific system gives the actual mass of the ionized compounds, the Waters system is calibrated to give the mass of the neutral compounds. This was considered when calculating the  $m/z$  values for comparison with the measurements.

UV-vis absorption spectra were recorded on an Agilent Cary 60 UV-vis spectrophotometer at room temperature. The measurements were carried out with 5  $\mu\text{M}$  solutions in  $\text{CHCl}_3$  at a scan rate of 300  $\text{nm min}^{-1}$  and a data interval of 0.5 nm. The baseline was corrected for plotting the data in Figure 5. Photoluminescence (PL) spectra were acquired on an Agilent Cary Eclipse fluorescence spectrophotometer with 5  $\mu\text{M}$  solutions in  $\text{CHCl}_3$  at a scan rate of 120  $\text{nm min}^{-1}$  and a data interval of 1 nm. The excitation and emission slits were set to 5 nm, the emission and excitation filters were set to 'auto' setting, and the detector voltage was set to 'high' (800 V). To facilitate a comparison, these are the same settings as used in our previous work on a set of ester-substituted macrocycles<sup>6</sup>.

Cyclic voltammetry (CV) measurements were carried out at arbitrary concentration using a glassy carbon working electrode, a platinum mesh auxiliary electrode, and a silver wire quasi-reference electrode (QRE) at a scan rate of 0.1  $\text{V s}^{-1}$ . 0.1 M Tetrabutylammonium hexafluorophosphate ( $\text{NBu}_4\text{PF}_6$ ) in dichloroethane (DCE) or dimethylformamide (DMF) were used as the supporting electrolyte solution. Ferrocene (Fc) was measured as reference. The solutions were purged with nitrogen for 5 min prior to the measurements. However, the presences of a reduction process at around -1.4 V vs.  $\text{Fc}/\text{Fc}^+$  in the measurements suggests that some residual oxygen was not efficiently removed by the purging process<sup>20</sup>. This reduction process was also present when measuring the supporting electrolyte solutions only (without a sample), corroborating that the process does not involve the macrocycles. In line with best practice, the redox potentials were estimated from the half-wave potential ( $E^{1/2}$ ) when reversibility was observed and from the inflection-point potential ( $E^i$ ) when no reversibility was observed<sup>21</sup>.

### Computational methods

Geometries for the neutral  $S_0$  and  $T_1$  states as well as the dianion and dication were optimized in vacuum using density functional theory (DFT) with the PBE0 functional<sup>22,23</sup> along with the def2-SV(P) basis set<sup>24</sup> and the D3 dispersion correction<sup>25</sup> in its optimised power version<sup>26</sup>. Transition state (TS) energies were optimized via a constrained optimization, fixing two of the phenylene-vinylene torsion angles, considering that a full TS optimization did not converge for **S-PCT** and verifying that the energies between this method and the full optimization were consistent for **O-PCT**. Interconversion times ( $t$ ) between rotamers were estimated via the Eyring equation

$$\frac{1}{t} = \frac{kT}{h} \exp\left(-\frac{\Delta_a E}{kT}\right)$$

where  $k$  and  $h$  are the Boltzmann and Planck constants,  $T = 298 \text{ K}$  is the temperature and  $\Delta_a E$  is the computed activation barrier. Redox potentials were computed using the PBE0 functional along with the def2-SVPD basis set using a conductor-like polarizable continuum model<sup>27</sup> considering a dielectric constant of 10.125 to represent 1,2-dichloroethane (DCE) and following the procedure described in detail in Ref. 6. All these computations were carried out in Q-Chem 5.3<sup>28,29</sup>.  $S_1$  states were optimised using time-dependent (TD) DFT with the  $\omega$ PBEh functional<sup>30</sup> (using  $\omega=0.1$  a.u. and 20% global Hartree-Fock exchange) along with the def2-SV(P) basis set and the D3 dispersion correction using the same D3-parameters as for PBE0.

Chemical shielding tensors were computed at the PBE0/def2-SVP level using gauge including atomic orbitals<sup>31</sup> as implemented in Gaussian 09<sup>32</sup>. Shielding tensors were represented graphically using the VIST (visualisation of chemical shielding tensors) method<sup>14</sup> as implemented in TheoDORE 2.4<sup>33</sup> using cclib<sup>34</sup> for some of the file parsing work and VMD<sup>35</sup> for the final graphical representation.

NDOs<sup>16</sup> for the  $T_1$  and charged states were computed using TheoDORE following two independent DFT calculations. NDOs for the  $S_1$  state were computed directly within Q-Chem after the TDDFT computation.

### Data availability

#### Underlying data

Zenodo: Research data for “[2.2.2.2]Paracyclophanetetraenes (PCTs): cyclic structural analogues of poly(p-phenylene vinylene)s (PPVs)”. <https://doi.org/10.5281/zenodo.5206265><sup>36</sup>

This project contains the following data:

- The underlying experimental research data ( $^1\text{H}$  NMR,  $^{13}\text{C}$  NMR,  $^{31}\text{P}$  NMR, high-resolution mass spectrometry (HRMS), UV-vis absorption, photoluminescence (PL), cyclic voltammetry)
- The underlying computational research data (molecular geometries, input/output files for Q-Chem, Gaussian, and TheoDORE)

Data are available under the terms of the [Creative Commons Attribution 4.0 International license](#) (CC-BY 4.0).

The  $^1\text{H}$  NMR,  $^{13}\text{C}$  NMR, and  $^{31}\text{P}$  NMR spectra are also available via ChemSpider. See CSIDs: 120300 (**S-2**), 3332510 (**O-3**), 110417237 (**S-3**), 110417244 (**O-P1**), 110417245 (**S-P1**), 14757439 (**Br-P2**), 110417240 (**S-P2**), 110417241 (**O-PCT**), and 110417242 (**S-PCT**).

### Acknowledgements

We thank Ugurcan Sal for contributing to synthetic experiments, Lisa Haigh for HRMS measurements, and Peter Haycock for NMR measurements at elevated temperature (all Imperial College London).

## References

- Blayney AJ, Perepichka IF, Wudl F, *et al.*: **Advances and Challenges in the Synthesis of Poly(*p*-phenylene vinylene)-Based Polymers.** *Isr J Chem.* 2014; 54(5–6): 674–688.  
[Publisher Full Text](#)
- Schönbein AK, Wagner M, Blom PWM, *et al.*: **Quantifying the Kinetics of the Gilch Polymerization toward Alkoxy-Substituted Poly(*p*-phenylene vinylene).** *Macromolecules.* 2017; 50(13): 4952–4961.  
[Publisher Full Text](#)
- Rimmele M, Ableidinger K, Marsh AV, *et al.*: **Thioalkyl- and sulfone-substituted poly(*p*-phenylene vinylene)s.** *Polym Chem.* 2019; 10(6): 738–750.  
[Publisher Full Text](#)
- Thulin B, Wennerström O, Högberg HE: **Simple Synthesis of [2.2.2]-Paracyclophane-1,9,17,25-Tetraene by a Wittig Reaction.** *Acta Chem Scand Ser B.* 1975; 29(1): 138–139.  
[Publisher Full Text](#)
- Eder S, Yoo DJ, Nogala W, *et al.*: **Switching between Local and Global Aromaticity in a Conjugated Macrocycle for High-Performance Organic Sodium-Ion Battery Anodes.** *Angew Chem Int Ed.* 2020; 59(31): 12958–12964.  
[PubMed Abstract](#) | [Publisher Full Text](#) | [Free Full Text](#)
- Rimmele M, Nogala W, Seif-Eddine M, *et al.*: **Functional group introduction and aromatic unit variation in a set of  $\pi$ -conjugated macrocycles: revealing the central role of local and global aromaticity.** *Org Chem Front.* 2021; 8(17): 4730–4745.  
[PubMed Abstract](#) | [Publisher Full Text](#) | [Free Full Text](#)
- Amal Joseph PJ, Priyadarshini S, Kantam ML, *et al.*: **Investigation of the scope and mechanism of copper catalyzed regioselective methylthiolation of aryl halides.** *Tetrahedron.* 2013; 69(38): 8276–8283.  
[Publisher Full Text](#)
- Prusinowska N, Bardziński M, Janiak A, *et al.*: **Sterically Crowded Trianglimines-Synthesis, Structure, Solid-State Self-Assembly, and Unexpected Chiroptical Properties.** *Chem Asian J.* 2018; 13(18): 2691–2699.  
[PubMed Abstract](#) | [Publisher Full Text](#)
- Yamamoto T, Nishimura T, Mori T, *et al.*: **Largely  $\pi$ -Extended Thienoacenes with Internal Thieno[3,2-*b*]thiophene Substructures: Synthesis, Characterization, and Organic Field-Effect Transistor Applications.** *Org Lett.* 2012; 14(18): 4914–4917.  
[PubMed Abstract](#) | [Publisher Full Text](#)
- Szakács Z, Glöckhofer F, Plasser F, *et al.*: **Excited-state symmetry breaking in 9,10-dicyanoanthracene-based quadrupolar molecules: the effect of donor-acceptor branch length.** *Phys Chem Chem Phys.* 2021; 23(28): 15150–15158.  
[PubMed Abstract](#) | [Publisher Full Text](#) | [Free Full Text](#)
- Gierschner J, Mack HG, Lürer L, *et al.*: **Fluorescence and absorption spectra of oligophenylenevinyls: Vibronic coupling, band shapes, and solvatochromism.** *J Chem Phys.* 2002; 116(19): 8596–8609.  
[Publisher Full Text](#)
- Su WF, Yeh KM, Chen Y: **Synthesis and optoelectronic properties of luminescent poly(*p*-phenylenevinylene) derivatives containing electron-transporting 1,3,4-oxadiazole groups.** *J Polym Sci Part A Polym Chem.* 2007; 45(18): 4377–4388.  
[Publisher Full Text](#)
- Kotani R, Liu L, Kumar P, *et al.*: **Controlling the S<sub>1</sub> Energy Profile by Tuning Excited-State Aromaticity.** *J Am Chem Soc.* 2020; 142(35): 14985–14992.  
[PubMed Abstract](#) | [Publisher Full Text](#)
- Plasser F, Glöckhofer F: **Visualisation of Chemical Shielding Tensors (VIST) to Elucidate Aromaticity and Antiaromaticity.** *Eur J Org Chem.* 2021; 2021(17): 2529–2539.  
[PubMed Abstract](#) | [Publisher Full Text](#) | [Free Full Text](#)
- Chen Z, Wannere CS, Corminboeuf C, *et al.*: **Nucleus-Independent Chemical Shifts (NICS) as an Aromaticity Criterion.** *Chem Rev.* 2005; 105(10): 3842–3888.  
[PubMed Abstract](#) | [Publisher Full Text](#)
- Plasser F, Wormit M, Dreuw A: **New tools for the systematic analysis and visualization of electronic excitations. I. Formalism.** *J Chem Phys.* 2014; 141(2): 024106.  
[PubMed Abstract](#) | [Publisher Full Text](#)
- Plasser F: **Exploitation of Baird Aromaticity and Clar's Rule for Tuning the Triplet Energies of Polycyclic Aromatic Hydrocarbons.** *Chemistry.* 2021; 3(2): 532–549.  
[Publisher Full Text](#)
- Kotha S, Cheekatla SR, Lal S, *et al.*: **Pentacycloundecane (PCUD)-Based Cage Frameworks as Potential Energetic Materials: Syntheses and Characterization.** *Asian J Org Chem.* 2020; 9(12): 2116–2126.  
[Publisher Full Text](#)
- Meindl B, Pfennigbauer K, Stöger B, *et al.*: **Double Ring-Closing Approach for the Synthesis of 2,3,6,7-Substituted Anthracene Derivatives.** *J Org Chem.* 2020; 85(12): 8240–8244.  
[PubMed Abstract](#) | [Publisher Full Text](#)
- Elgrishi N, Rountree KJ, McCarthy BD, *et al.*: **A Practical Beginner's Guide to Cyclic Voltammetry.** *J Chem Educ.* 2018; 95(2): 197–206.  
[Publisher Full Text](#)
- Espinoza EM, Clark JA, Soliman J, *et al.*: **Practical Aspects of Cyclic Voltammetry: How to Estimate Reduction Potentials When Irreversibility Prevails.** *J Electrochem Soc.* 2019; 166(5): H3175–H3187.  
[Publisher Full Text](#)
- Perdew JP, Burke K, Ernzerhof M: **Generalized Gradient Approximation Made Simple.** *Phys Rev Lett.* 1996; 77(18): 3865–3868.  
[PubMed Abstract](#) | [Publisher Full Text](#)
- Adamo C, Barone V: **Toward reliable density functional methods without adjustable parameters: The PBE0 model.** *J Chem Phys.* 1999; 110(13): 6158–6170.  
[Publisher Full Text](#)
- Weigend F, Ahlrichs R: **Balanced basis sets of split valence, triple zeta valence and quadruple zeta valence quality for H to Rn: Design and assessment of accuracy.** *Phys Chem Chem Phys.* 2005; 7(18): 3297–3305.  
[PubMed Abstract](#) | [Publisher Full Text](#)
- Grimme S, Antony J, Ehrlich S, *et al.*: **A consistent and accurate *ab initio* parametrization of density functional dispersion correction (DFT-D) for the 94 elements H-Pu.** *J Chem Phys.* 2010; 132(15): 154104.  
[PubMed Abstract](#) | [Publisher Full Text](#)
- Witte J, Mardirossian N, Neaton JB, *et al.*: **Assessing DFT-D3 Damping Functions Across Widely Used Density Functionals: Can We Do Better?** *J Chem Theory Comput.* 2017; 13(5): 2043–2052.  
[PubMed Abstract](#) | [Publisher Full Text](#)
- Barone V, Cossi M: **Quantum Calculation of Molecular Energies and Energy Gradients in Solution by a Conductor Solvent Model.** *J Phys Chem A.* 1998; 102(11): 1995–2001.  
[Publisher Full Text](#)
- Shao Y, Gan Z, Epifanovsky E, *et al.*: **Advances in molecular quantum chemistry contained in the Q-Chem 4 program package.** *Mol Phys.* 2015; 113(2): 184–215.  
[Publisher Full Text](#)
- Krylov AI, Gill PMW: **Q-Chem: an engine for innovation.** *Wiley Interdiscip Res Comput Mol Sci.* 2013; 3(3): 317–326.  
[Publisher Full Text](#)
- Rohrdanz MA, Martins KM, Herbert JM: **A long-range-corrected density functional that performs well for both ground-state properties and time-dependent density functional theory excitation energies, including charge-transfer excited states.** *J Chem Phys.* 2009; 130(5): 054112.  
[PubMed Abstract](#) | [Publisher Full Text](#)
- Cheeseman JR, Trucks GW, Keith TA, *et al.*: **A comparison of models for calculating nuclear magnetic resonance shielding tensors.** *J Chem Phys.* 1996; 104(14): 5497–5509.  
[Publisher Full Text](#)
- Frisch MJ, Trucks GW, Schlegel HB, *et al.*: **Gaussian 09, Revision E.01.** Wallingford, CT, 2013.
- Plasser F: **TheoDOR: A toolbox for a detailed and automated analysis of electronic excited state computations.** *J Chem Phys.* 2020; 152(8): 084108.  
[PubMed Abstract](#) | [Publisher Full Text](#)
- O'boyle NM, Tenderholt AL, Langner KM: **cclib: A library for package-independent computational chemistry algorithms.** *J Comput Chem.* 2008; 29(5): 839–845.  
[PubMed Abstract](#) | [Publisher Full Text](#)
- Humphrey W, Dalke A, Schulten K: **VMD: visual molecular dynamics.** *J Mol Graph.* 1996; 14(1): 33–38, 27–8.  
[PubMed Abstract](#) | [Publisher Full Text](#)
- Pletzer M, Plasser F, Rimmele M, *et al.*: **Research data for "[2.2.2]Paracyclophanetetraenes (PCTs): cyclic structural analogues of poly(*p*-phenylene vinylene)s (PPVs)".** [Data set]. *Zenodo.* 2021. <http://www.doi.org/10.5281/zenodo.5206265>